

Inhibition and promotion of electrochemical reactions by graphene in organic coatings

A. U. Chaudhry,^a Vikas Mittal^b and Brajendra Mishra^a

Supplementary information

Synthesis of PVB/GP Composite Coatings

Materials. Polyvinyl butyral (PVB) with trade name Butvar B-98 (molecular weight 40,000-70,000) and sodium dodecyl sulfate (SDS) were purchased from Sigma Aldrich. PVB had 18-20% hydroxyl content, and 80% butyral content. Graphene nano-powder was provided by Graphene Supermarket, USA. The sample had particles with average thickness < 3nm (between 3-8 graphene monolayers) and lateral dimensions 2-8 μm .

Model coatings were prepared by dissolving PVB (Figure S1) 2000 ppm (0.2 wt. % of methanol weight) and SDS 300ppm (0.03 wt. % of methanol weight) in 50 mL (39.6 g) methanol with continuous stirring for 24 h, followed by sonication in a sonicator bath. SDS was used as dispersant and used in all coatings. Similarly, two different concentrations of GP powder i.e. 1000 ppm (0.1 wt. % of methanol weight) and 2000 ppm (0.2 wt. % of methanol weight) was subjected to sonication in 50 mL (39.6 g) methanol with 300 ppm (0.03 wt. % of methanol weight) SDS for 1 h. PVB was added to the GP dispersion and shaken for 72 h to generate a uniform dispersion of GP in the PVB solution¹. Using dip coater (Figure S5), carbon steel substrates were coated with PVB-GP dispersion by immersion and withdraw speed of 50 and 200 mm/min respectively. Samples were immersed in solution for 1 min. Three coats were applied for each sample in similar manner with an interval of 20 min. Further, the samples were dried at room temperature for 3 d followed by baking in air circulating oven at 175°C for 2 h to generate final coating with thickness in the range of 70 \pm 3 μm (Figure S6).

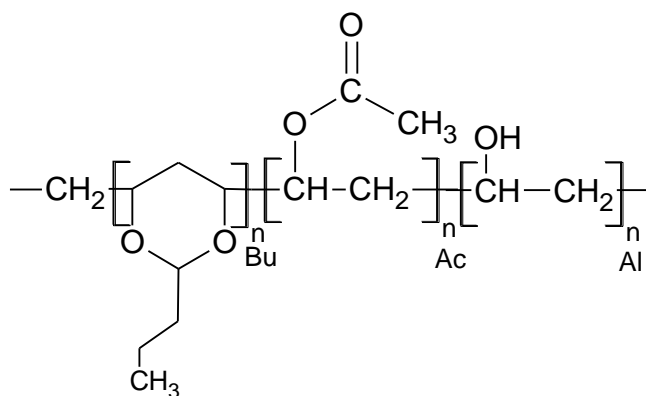


Figure S1. Structure of Butvar B-98 (Bu: Butyral, Ac: Acetate, Al: Alcohol)

Electrochemical Characterization

Electrochemical Procedure A flat cell assembly with working volume of 250 mL (Figure S2), consisting of carbon steel coupon as the working electrode (WE) with expose area 2.6 cm^2 , graphite plate as counter electrode (CE) having dimensions of $25 \times 25 \times 5 \text{ mm}$ with expose area 2.6 cm^2 , and a silver/silver chloride electrode as reference electrode (RE), were used for the electrochemical measurements. Carbon steel panels were surface finished using different grades of SiC grit papers from 240 up to 600 grit, polished to a mirror finish followed by cleaning and degreasing with industrial grade acetone and drying in air. Before coating, specimen were treated with 2% nital for 1 min and used immediately without any further treatment.

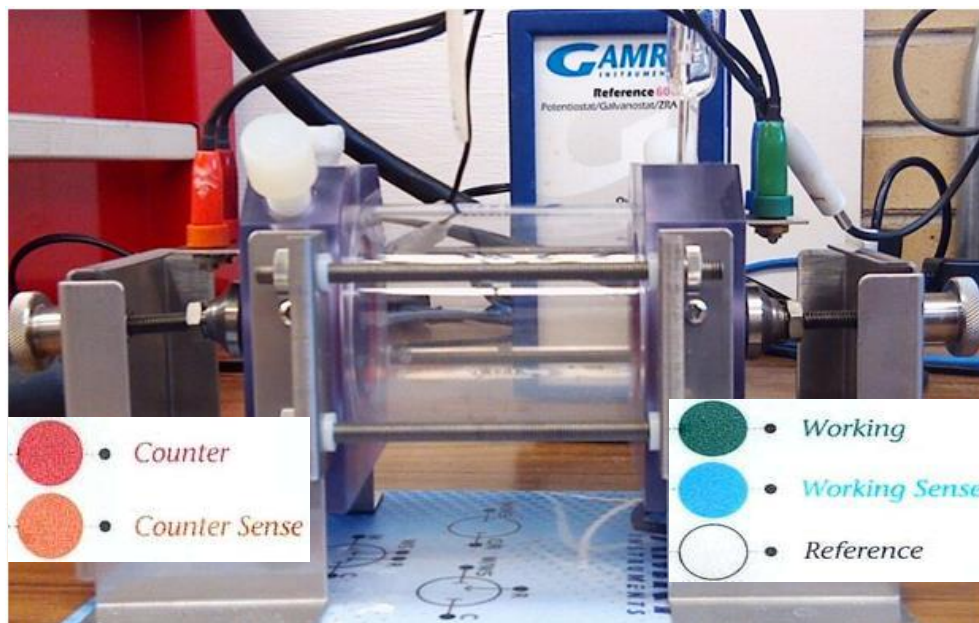
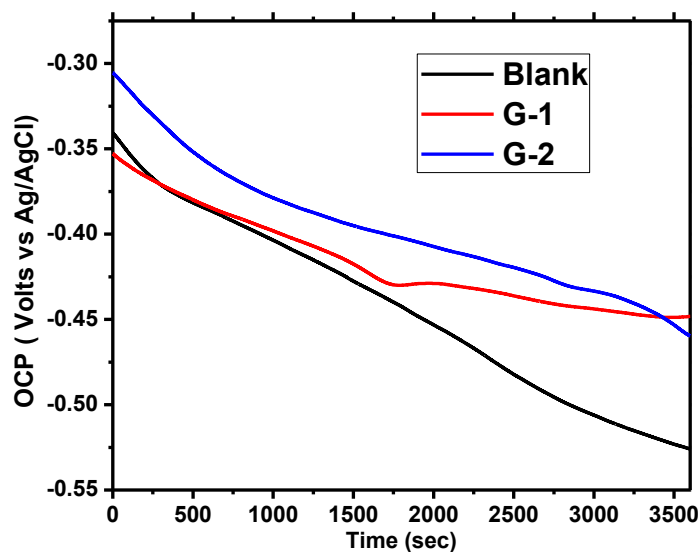


Figure S2. Electrochemical flat cell Setup

Electrochemical testing was performed in a closed system under naturally aerated conditions using a Gamry 600 potentiostat/galvanostat/ZRA at room temperature. The sequence of electrochemical techniques is described below. Corrosion studies were carried out in 0.1 M NaCl conditions.

Open Circuit Potential (OCP). The open circuit potential of steel samples was recorded against Ag/AgCl electrode as reference electrode for 1 and 26 h, in solutions of 0.1M NaCl (Figure S3). After the completion of each step, EIS was measured followed by final potentiodynamic measurements by closely following the ref².



a



b

Figure S3. Open circuit potential after 1 h (a) and 26 h (b) of immersion in 0.1M NaCl

Electrochemical Impedance Spectroscopy (EIS). Impedance measurements were performed as a function of open circuit potential (E_{OCP}) at 1 and 26 h from the time of immersion. The frequency sweep was performed from 10^5 to 10^{-2} Hz at 10 mV AC amplitude. The Bode plots were modeled with mono-phasic circuit model used to fit EIS data as resistor and capacitors as shown in Figure S4(a-b), where. For the description of a frequency independent phase shift

between the applied AC potential and its corresponding current response, a constant phase element (CPE) is used, where impedance of the CPE is given by,

$$Z(CPE) = Y_o^{-1} [j\omega]^{-n}$$

where, Y_o is the constant of CPE, ω is the angular frequency in rad s^{-1} and n is the exponential term which can vary between 1 for pure capacitance and 0 for a pure resistor³⁻⁶. n is a measure of surface in homogeneity; the lower is its value, the higher is the surface roughening of the metal/alloy⁶.

This circuit model simulates the structure of a barrier coating over the electrode surface and also explains the surface inhomogeneity or roughness. At 1 and 26 h, the alloy shows a one time constant impedance response for all samples. This behavior can be easily noticed in the phase angle Bode curves as a single hump for dominant one time constant phase. To simulate the electrochemical interface, EIS data was analyzed with Echem Analyst using circuit model having electrical equivalent parameters accordingly.

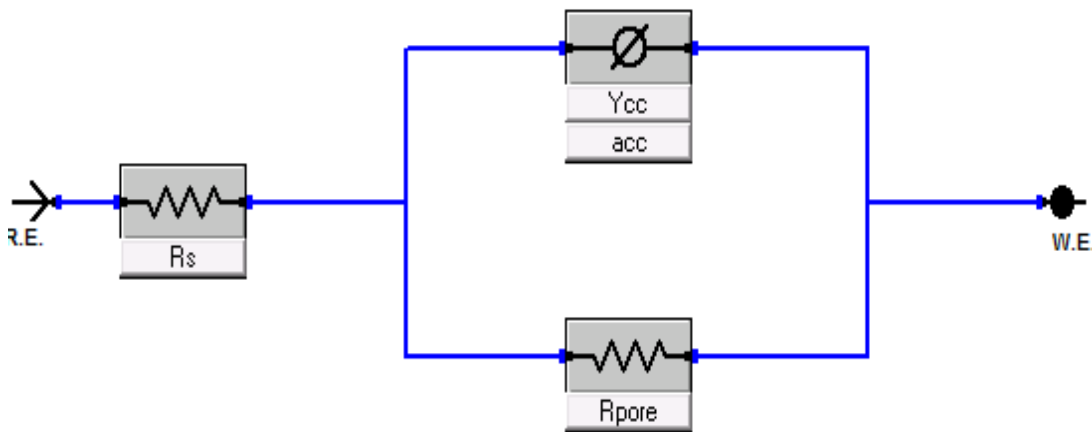
The capacitance C has been calculated using the following equation:

$$C = Y [j\omega'']^{n-1}$$

where ω'' is the frequency found at the maximum of the imaginary part of the impedance, Z'' . The resistance efficiency, ER has been calculated as indicated by equation⁵:

$$ER = \frac{[R' - R]}{R'}$$

where R' and R are the resistance value with and without GP respectively.



a

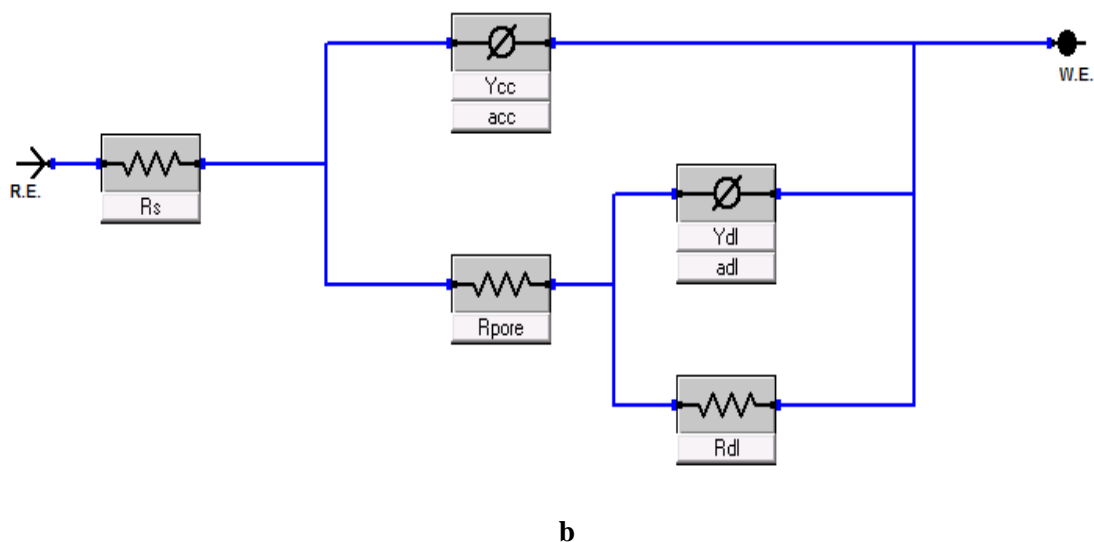


Figure S4. Circuit model after 1 hour a) and after 26 hour b) of immersion

Potentiodynamic Polarization (PD). The polarization measurements were performed at 26 h of immersion by polarizing the working electrode from an initial potential of -0.3 mV up to a final potential of 0.3 mV as a function of open circuit potential (E_{OCP}). A scan rate of 0.5 mV/s was used for the polarization sweep^{7,8}. Corrosion current densities i_{corr} were obtained by extrapolating anodic and cathodic linear segments of Tafel plot using Echem Analyst. The obtained current densities were used to calculate the efficiency of corrosion inhibition using the following equation⁵:

$$CE = \left[\frac{i_{corr} - i'_{corr}}{i_{corr}} \right]$$

where i_{corr} and i'_{corr} are the current densities without and with the GP.



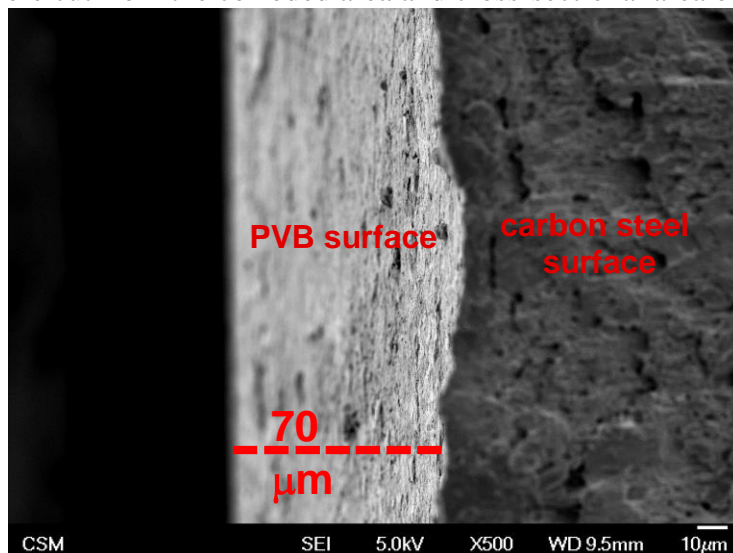
Figure S5. Dip Coater

Coatings and Materials Characterization

Transmission Electron Microscopy (TEM) imaging was performed to characterize the GP. FEI Philips C200 TEM with 200 kV was used. The samples were prepared by dispersing approximately 1 mg of GP in 10 mL of acetone and sonicating for 30 min in a water bath at room temperature. One drop of the suspension was then deposited on a 400-mesh copper grid covered with thin amorphous film to view under the microscope.

JEOL JSM-7000F field emission scanning electron microscope (FE-SEM) was used to evaluate coating morphology at different kV under high vacuum at a working distance of 10 mm. Coated

samples were cut from the corroded area and cross-sectional area of coating was observed as



shown by

Figure S6.

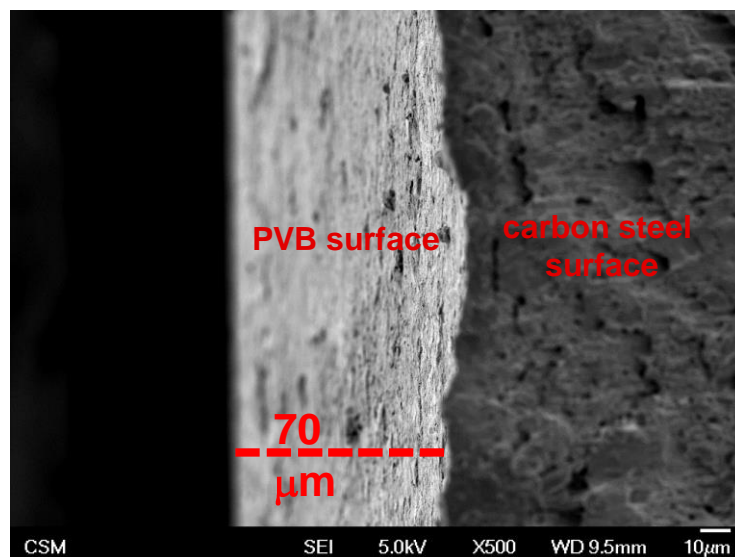


Figure S6. Cross-sectional area showing metal-coating interface

X-ray diffraction (XRD) measurements were performed to confirm the GP by comparing it with graphite. Philips PW 3040/60 spectrometer using Cu K α radiation in range of 10° to 40° at scan rate 0.050° was used and the diffraction peaks were matched using X'Pert HighScore software.

Thermo-Electron Nicolet 4700 FTIR spectrometer was used for measurements using ATR reflection mode. The IR spectra of PVB and composites films were taken using ZnSe crystal between 4000 cm⁻¹ and 600 cm⁻¹.

Thermogravimetric analyzer (TGA) was used to record the thermal degradation properties of GP and PVB. Nitrogen was used as a carrier gas and the scans were obtained for different temperature using a heating rate of 20 °C/min

TA Instruments Q20 differential scanning calorimeter (DSC) was used to measure the calorimetric properties of PVB under nitrogen atmosphere. First scans were obtained from 25–175°C using heating rate of 15 °C/min. Before second heating, the samples were also heated isothermally at 200 °C for 2 h and scanned again from 25-175 °C to detect the variations in glass transition temperature (T_g) upon heating.

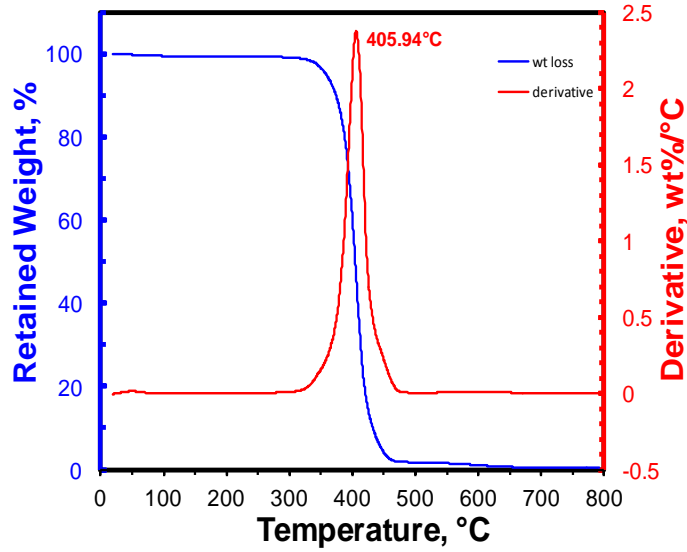
Raman spectra were taken using procedure earlier done⁹. Briefly, small amount of GP powder was compressed between glass slides to acquire GnP layer. One of the glass slide was placed under the spectrometer objective with magnification of $\times 50$ and the spectra of these layers were recorded using LabRAM HR. The charge-coupled device (CCD) exposure time was 20 s, and an average of 10 cycles was used to increase S/N ratio. Raman shifts were calibrated with the silicon reference peak at 520.7 cm^{-1} . Raman mapping was conducted in Duoscan mode on an array size of 23 $\mu\text{m} \times 18 \mu\text{m}$. Each spot size was 2 μm , and spectra were collected using an exposure time of 5 s and 1 cycle.

Results

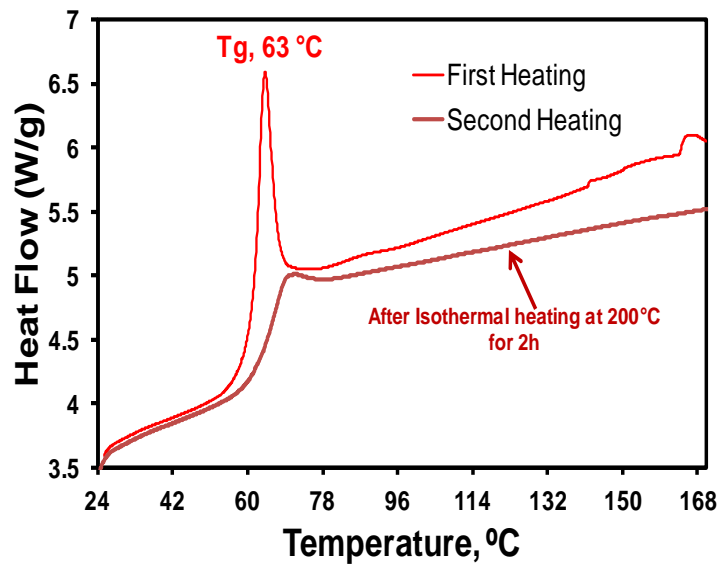
PVB Characterization

TGA (nitrogen) (Figure S7a) demonstrates the thermal degradation of PVB resin over temperature range of 20-800 °C. The weight loss of 9% up to 370°C can be observed due to the dehydration of copolymer. The degradation peak around 406°C indicates the major thermal degradation (89%) of PVB which continues till 460°C, liberating products such as butanal, C4-hydrocarbons followed by degradation of cyclic and crosslinked compounds¹⁰.

Figure S7b depicts the DSC thermograms of PVB before and after isothermal heating. First heating clearly indicates the presence of sharp peak at 63°C indicating glass transition temperature (T_g). After isothermal heating at 200°C for 2 hrs, second heating indicates disappearance of sharp peak and shows a small hump in the thermogram at 70 °C. This behavior was unlike to the previous reports where thermal treatment showed that T_g shifted to 170°C It was reported that the self-crosslinking of PVB was taking place owing to the interaction of -OH or acetate groups on adjacent PVB chains which may results reactions between functional groups leading the bridge bonds¹¹.



a



b

Figure S7. TGA a) and DSC b) thermograms of PVB

Figure S8 and Table S1 show the infrared spectroscopy spectra and analysis of assigned peaks. The spectrum of heat treated resin does not show any new peak indicating absence of new bonds owing to cross-linking. These results are in agreement with the previous reports where heat treatment produced changes in PVB structure measured by hardening of sample¹². Similarly, GP IR spectrum does not confirm the presence of any functional group at surface and no new peak was observed in case of PVB and GP composites.

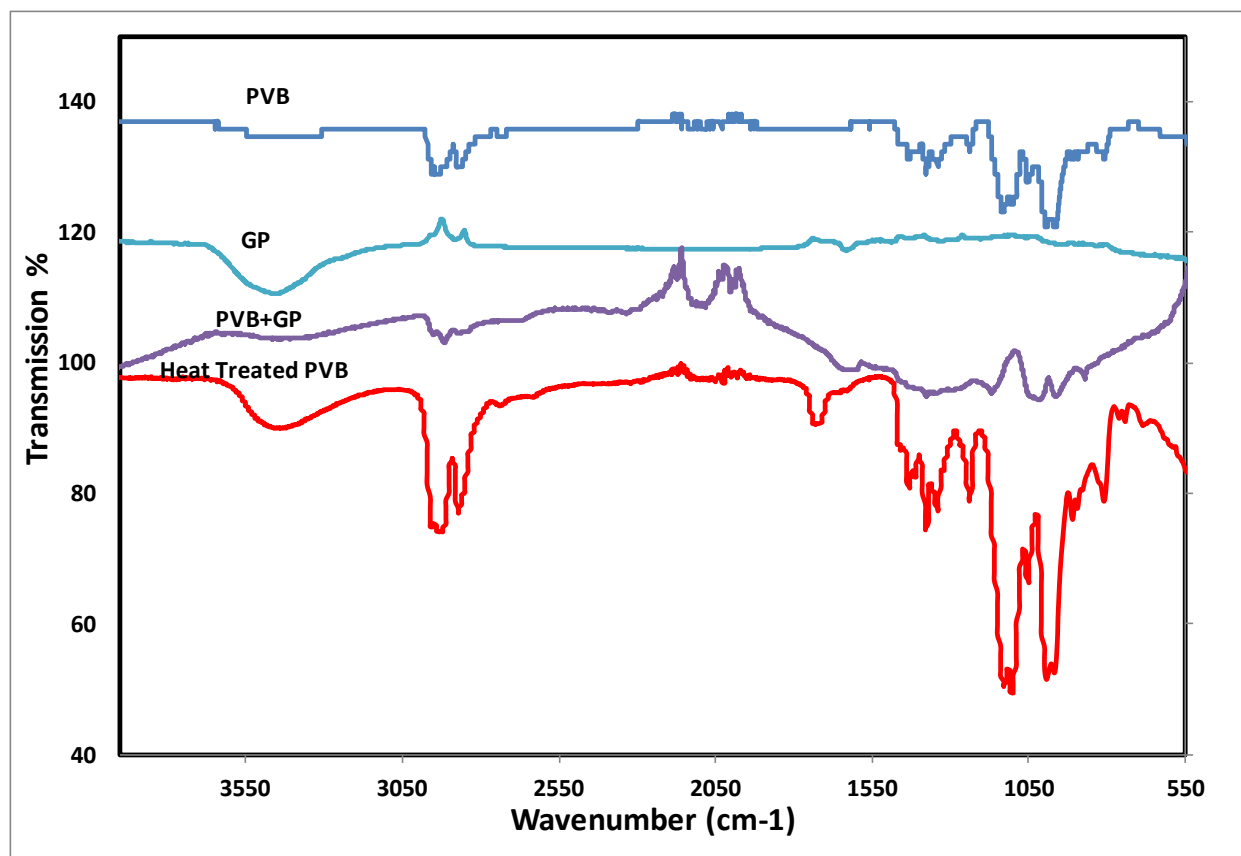


Figure S8. FT-IR spectrums

Table S1. FTIR analysis of PVB and cross linked PVB

Group frequency PVB	Assg.	Cross-linked PVB	Assg.	GP	Assg.	PVB+GP	Assg.
3454	-OH asymmetric stretching of polyvinyl alcohol	3435	-OH asymmetric stretching of polyvinyl alcohol	3456	stretching and bending of the OH bond	2918	asymmetric -CH ₂ stretching
2939	asymmetric -CH ₂ stretching	2933	asymmetric -CH ₂ stretching	2881	C-H stretching vibration	2172	Acetal
2869	Symmetric -CH ₂ stretching	2870	Symmetric -CH ₂ stretching	2043	C=C stretching vibration	2083	CC stretching vibration
2740	O=C-H	1732	carbonyl	1633	Graphitic	2003	asymmetric

	stretching (Aldehyde group)		stretching of the acetate		C=C π - bonds		C=C stretching vibration
1733	carbonyl stretching of the acetate	1433	-CH ₂ bending	1338- 1203	C-H deformation vibration		
1438	-CH ₂ bending	1379	C-H bending vibration			1377	C-H bending vibration
1377- 1337	C-H bending vibration	1342	C-H bending vibration			1013	C-O-C- O-C stretching vibrations of cyclic acetal groups
1316- 1236	C-O stretching vibration of acetate group	1239	C-O stretching vibration of acetate group				
1136 -998	C-O-C- O-C stretching vibrations of cyclic acetal groups	1130- 994	C-O-C-O-C stretching vibrations of cyclic acetal groups				

GP Characterization

The bulk conductivity of the GP sheet was found to be $5.78 \times 10^{+03}$ S/m which was measured using four probe methods and has good agreement with published literature¹³. The GP sheet was obtained by pressing powder GP in a sheet form on Teflon sheet using 10 lb_f for 5 min. The sheet bulk resistance was measured using four probe methods at different areas on GP sheet using 200 mV and 4.53×10^{-03} Ampere. The conductivity of sheet was calculated according to following equations:

$$\rho(\Omega.m) = R_s(\text{sheet resistance}, \frac{\Omega}{\square}) \times T_s(\text{sheet thickness}, m)$$

$$\sigma \left(\text{conductivity}, \frac{S}{m} \right) = \frac{1}{\rho(\Omega \cdot m)}$$

Figure S9 shows characteristic low-resolution TEM images of graphene nanoplatelets (sheets) showing flaky and transparent structure with wrinkles and folding on the surface ¹⁴.

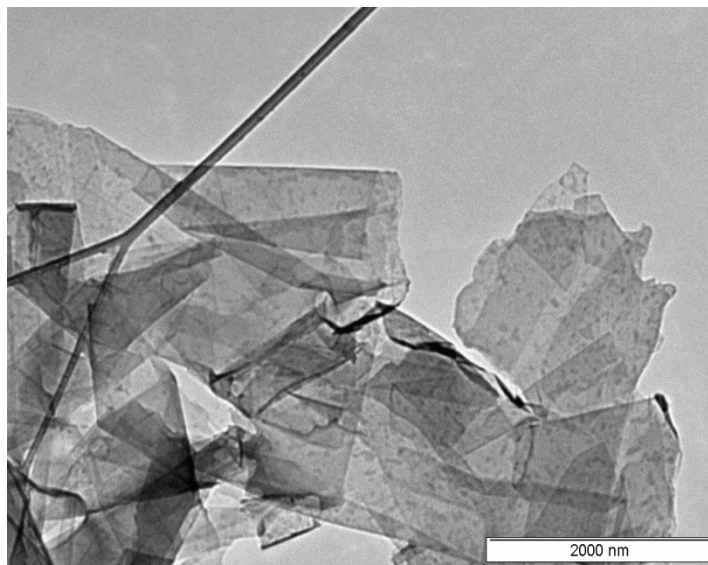


Figure S9. TEM of an aggregate consisting of a folded graphene nanoplatelets

Figure S10 shows the TGA thermogram of GP from 50 to 650°C under nitrogen. A very small weight loss in GP may be attributed to the adsorbed water molecules entrapped in graphene stacked galleries since GP has stacked structure as shown in XRD profile (Figure S11) ¹⁵.

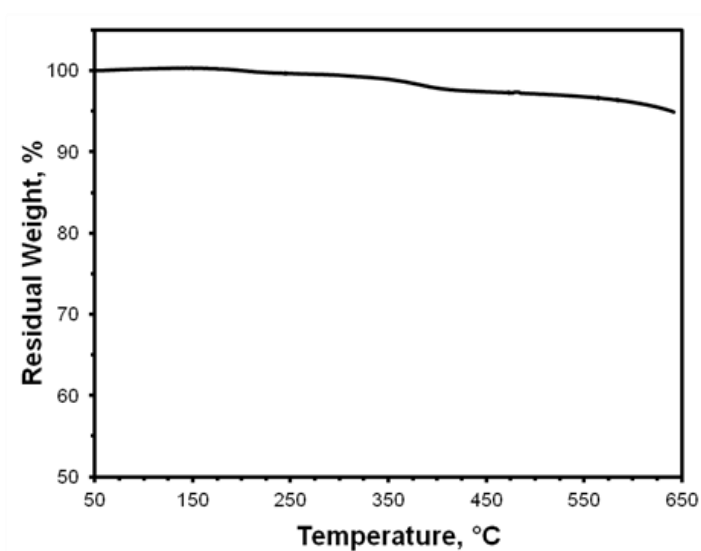


Figure S10. Thermogravimetric curve for graphene nanoplatelets

Figure S11 depicts XRD profile of graphite and GP. The characteristic peak at $2\theta \sim 26.5^\circ$ represents the 002 plane in hexagonal graphite with interlayer spacing of 0.334 nm. For XRD profile of GP, the sharp peak of graphite at $2\theta \sim 26.5^\circ$ disappeared indicating the exfoliated graphene layers¹⁶.

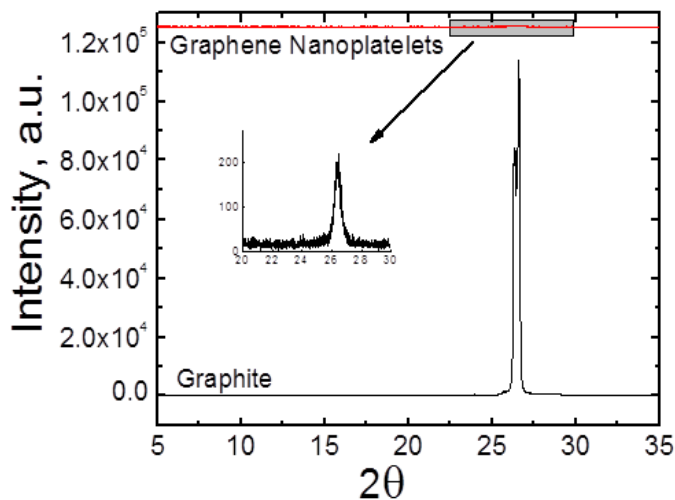


Figure S11. XRD profile of graphite and GP

Coating morphology

Figure 12 shows the FE-SEM images of sandwich like morphological structure of GP-PVB composites. The lateral dimension of graphene as provided and also confirmed by TEM (Figure S9) was about 2-8 microns. The thickness of the GP stacks in coatings was varying and uniformly distributed. Most of the stacks found to be < 50 nm and except for few which were < 100 nm indicating extensive exfoliation of graphene sheets¹⁷. The monolayer stacks size range indicates that that graphene is more or less dispersed in PVB coatings but effective enough to act as barrier for corrosive solution owing to large lateral size.

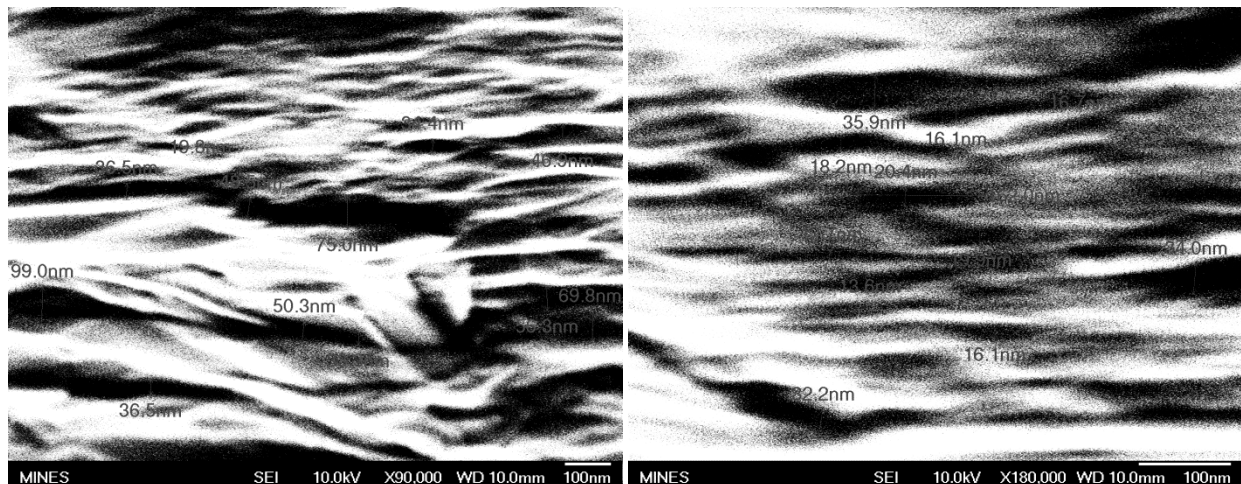


Figure 12 FE-SEM images of cross sections of coatings showing dispersion of GP in PVB for G-2 at 90 and 180 thousand of magnification

Raman characterization of GP

Figure 13 depicts common features of Raman spectrum for GP showing the presence of D band~1330(zone center phonons of E_{2g} symmetry), G band ~1560(K-point phonons of A_{1g} symmetry) and 2D band ~2650 cm^{-1} . D peaks corresponds the breathing modes of sp^2 rings¹⁸ and confirms the presence of defects in graphene. The much lower intensity of D peak as compare to G peak indicates high quality of graphene. The lower intensity of 2D peak as compare to D peak indicates presence of multiple graphene layers¹⁹.

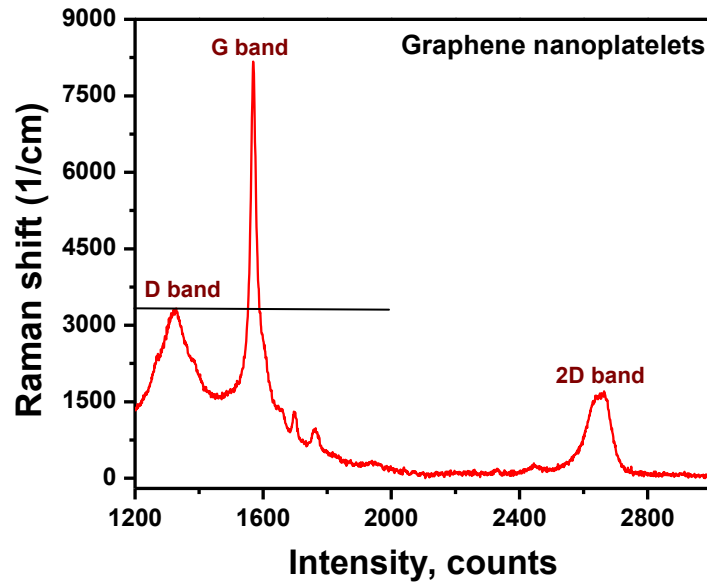


Figure 13 Raman spectrums for Graphene nanoplatelets (GP)

X-ray photoelectron spectroscopy of corroded surface

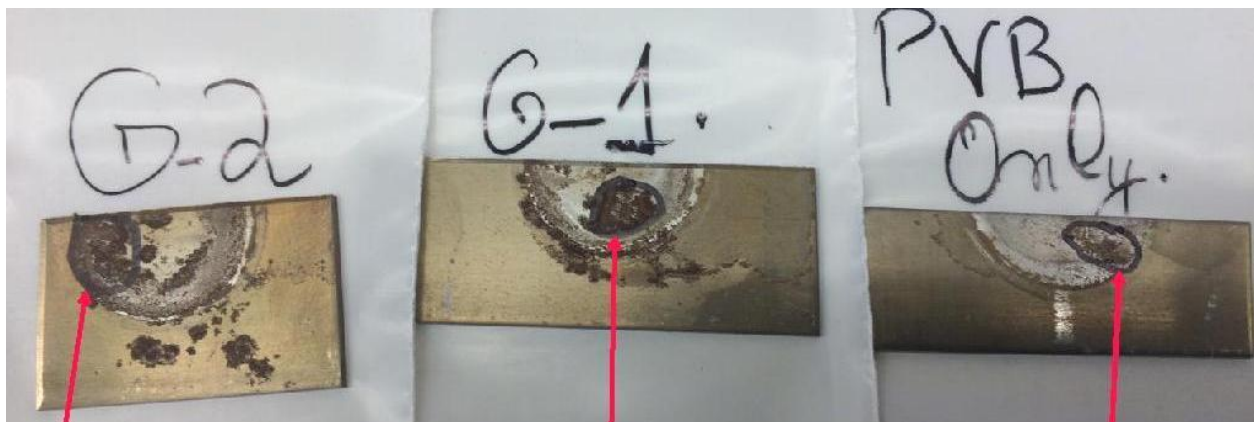


Figure 14. Images of corroded sample after treated with methanol, XPS were recorded somewhere in the encircle area

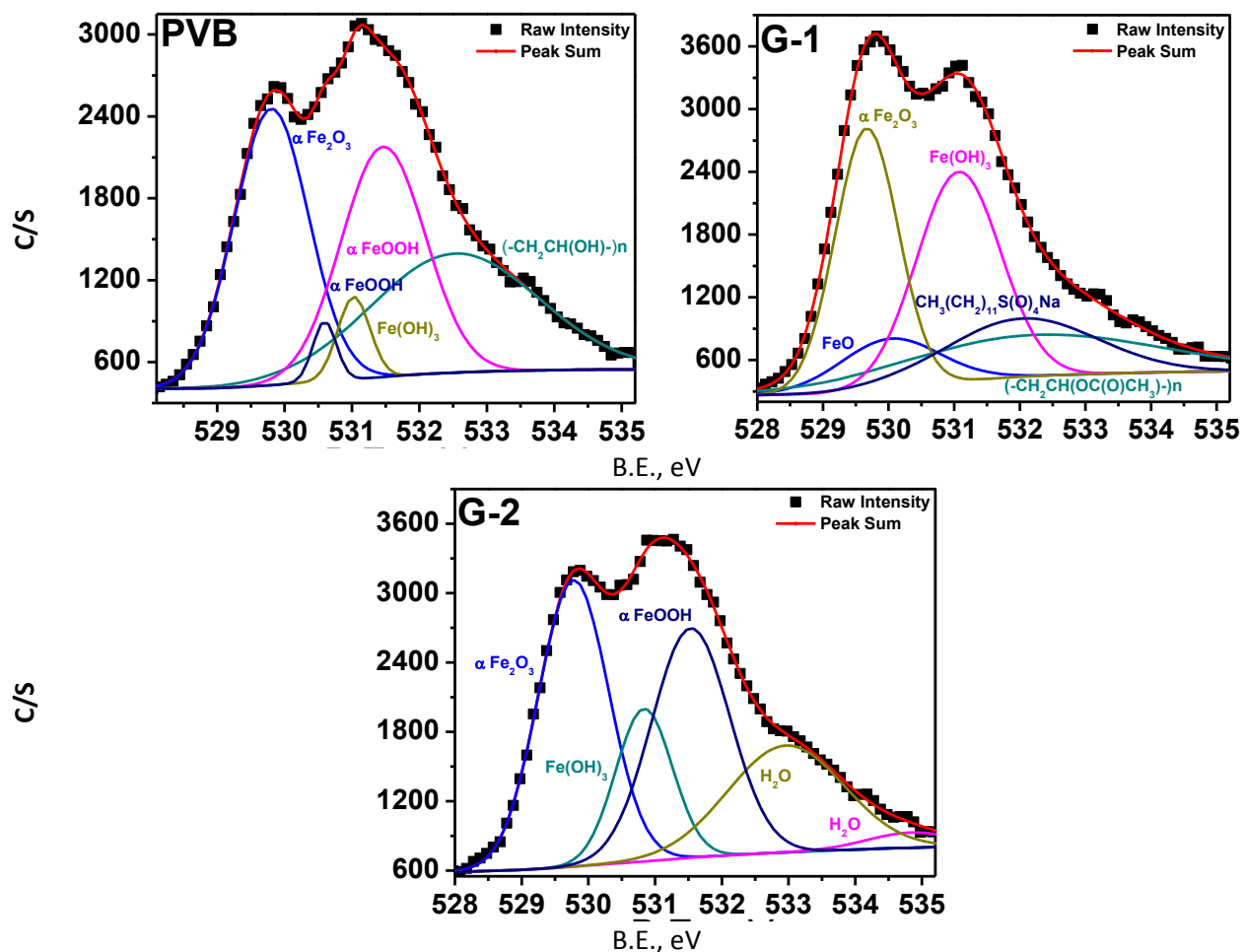


Figure 15 XPS spectra for O1s of corroded sample surface

References

1. S. Radhakrishnan, C. R. Siju, D. Mahanta, S. Patil and G. Madras, *Electrochimica Acta*, 2009, **54**, 1249-1254.
2. D. Asefi, M. Arami and N. M. Mahmoodi, *ECS Trans.*, 2011, **35**, 1-10.
3. S. M. Bholá, R. Bholá, B. Mishra and D. L. Olson, *J. Mater. Sci: Mater. in Med.*, 2011, **22**, 773-779.
4. C. Hsu and F. Mansfeld, *Corros.*, 2001, **57**, 747-748.
5. S. Sathiyarayanan, C. Jeyaprabha, S. Muralidharan and G. Venkatachari, *Appl. Surf. Sci.*, 2006, **252**, 8107-8112.
6. S. Chongdar, G. Gunasekaran and P. Kumar, *Electrochim. Acta*, 2005, **50**, 4655-4665.
7. ASTM-G61-86, *Journal*, 2009, DOI: 10.1520/G0061-86R09.
8. ASTM-G3-89, *Journal*, 2010, DOI: 10.1520/G0003.
9. V. Mittal, T. Akhtar, G. Luckachan and N. Matsko, *Colloid Polym Sci*, 2015, **293**, 573-585.
10. L. C. K. Liao, T. C. K. Yang and D. S. Viswanath, *Polymer Engineering & Science*, 1996, **36**, 2589-2600.
11. 2008.
12. K. E. Spirydowicz, E. Simpson, R. A. Blanchette, A. P. Schniewind, M. K. Toutloff and A. Murray, *Journal of the American Institute for Conservation*, 2001, **40**, 43-57.

13. W. Kundhikanjana, K. Lai, H. Wang, H. Dai, M. A. Kelly and Z.-x. Shen, *Nano Letters*, 2009, **9**, 3762-3765.
14. Y. Shao, S. Zhang, C. Wang, Z. Nie, J. Liu, Y. Wang and Y. Lin, *Journal of Power Sources*, 2010, **195**, 4600-4605.
15. H. Zheng, C. Y. Neo, X. Mei, J. Qiu and J. Ouyang, *Journal of Materials Chemistry*, 2012, **22**, 14465-14474.
16. K. Zhang, Y. Zhang and S. Wang, *Sci. Rep.*, 2013, **3**.
17. V. Mittal and A. U. Chaudhry, *Journal of Applied Polymer Science*, 2015, **132**.
18. C. Casiraghi, A. Hartschuh, H. Qian, S. Pisanec, C. Georgi, A. Fasoli, K. S. Novoselov, D. M. Basko and A. C. Ferrari, *Nano Letters*, 2009, **9**, 1433-1441.
19. A. Nieto, D. Lahiri and A. Agarwal, *Carbon*, 2012, **50**, 4068-4077.